Boron- and Nitrogen-Substituted Graphene Nanoribbons as Efficient Catalysts for Oxygen Reduction Reaction

ARTICLE *in* CHEMISTRY OF MATERIALS · FEBRUARY 2015

Impact Factor: 8.35 · DOI: 10.1021/cm5037502

CHEMISTRY OF MATERIALS

Article

pubs.acs.org/cm

Boron- and Nitrogen-Substituted Graphene Nanoribbons as Efficient Catalysts for Oxygen Reduction Reaction

Yongji Gong,[†,#] Huilong Fei,[†,#] Xiaolong Zou,[‡,#] Wu Zhou,[§] Shubin Yang,*[,‡,∥] Gonglan Ye,[‡] Zheng Liu,[‡] Zhiwei Peng,[†] Jun Lou,[‡] Robert Vajtai,[‡] Boris I. Yakobson,[†,‡] James M. Tour,*[,†,‡,⊥] and Pulickel M. Ajayan*[,†,‡]

[†]Department of Chemistry, [‡]Department of Materials Science & NanoEngineering, and [⊥]Smalley Institute for Nanoscale Science and Technology, Rice University, Houston, Texas 77005, United States

[§]Materials Science & Technology Division, Oak Ridge National Laboratory, Oak Ridge, Tennessee 37831, United States

[∥]School of Materials Science & Engineering, Beihang University, Beijing, 100191, China

Supporting Information

ABSTRACT: We show that nanoribbons of boron- and nitrogen-substituted graphene can be used as efficient electrocatalysts for the oxygen reduction reaction (ORR). Optimally doped graphene nanoribbons made into three-dimensional porous constructs exhibit the highest onset and half-wave potentials among the reported metal-free catalysts for this reaction and show superior performance compared to commercial Pt/C catalyst. Furthermore, this catalyst possesses high kinetic current density and four-electron transfer pathway with low hydrogen peroxide yield during the reaction. First-principles calculations suggest that such excellent electrocatalytic properties originate from the abundant edges of boron- and nitrogen-codoped graphene nanoribbons, which significantly reduce the energy barriers of the rate-determining steps of the ORR reaction.

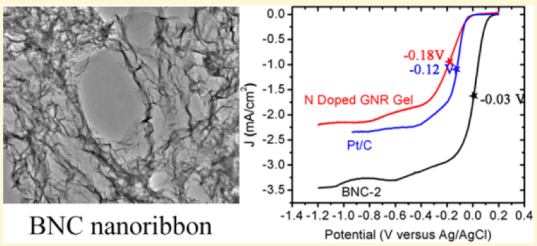

Due to the kinetic sluggishness of the oxygen reduction reaction (ORR) with the four-electron transfer pathway in the electrodes, developing new active electrocatalysts for ORR has recently become a key to boost the practical applications of fuel cells and metal−air batteries.[1−3] Although platinum (Pt) and its alloys exhibit high activity for ORR, their performance has been overshadowed by the high cost and scarcity of Pt and by the reduced thermal efficiency caused by substantial overpotential for the ORR.[4−6] Hence, intensive efforts have been devoted to substitute Pt-based catalysts by employing nonprecious metal catalysts and preferably metal-free catalysts. For instance, various heteroatom (nitrogen, sulfur, or phosphorus)-doped carbon nanotubes, mesoporous carbons, and graphene sheets have been widely explored for ORR catalysts via various synthesis approaches.[1,2,7−12] The research of designing new catalysts to reduce the overpotential and understanding the nature of ORR catalytic sites and mechanisms in metal-free catalysts is still in its infancy.[13−16]

In general, the adsorption of oxygen and formation of superoxide through a one-electron reduction on metal-free catalysts such as N-doped graphene sheets have been suggested as the initial ORR steps, and O_2 adsorption is proposed to be the rate-determining step.[17−19] Since oxygen is preferred to be adsorbed onto the exposed edges of N-doped graphene rather than the basal planes, it is clear that the edges of N-doped graphene-based catalysts possess high ORR activity while the basal planes remain virtually ORR inactive.[19] Thus, edge-abundant, nitrogen-doped graphene would facilitate the formation of catalytic sites for ORR. In this regard, unique carbon nanotube−nanoribbon complexes with controllable nitrogen doping have been recently explored via partially unzipping carbon nanotubes and subsequent annealing under NH_3 atmosphere, showing enhanced catalytic activity for ORR. However, in rotating-disk electrode (RDE) polarization studies, their ORR onset potentials and half-wave potentials ($E_{1/2}$) are still lower than those of commercially available Pt catalysts.[2] This would result in high overpotentials of fuel cells at practical operating current densities and cause low thermal efficiency.[6] Thus, developing new strategies to engineer efficient metal-free ORR catalysts still remains challenging.

Here, we develop an efficient approach to construct three-dimensional (3D) architectures from numerous edge-abundant boron- and nitrogen-substituted carbon nanoribbons (hitherto termed BNC NRs) for ORR electrocatalysts. The typical synthesis approach involves the use of graphene oxide nanoribbons (GONRs) as building blocks to construct 3D architectures and subsequent employment of boric acid and ammonia as boron and nitrogen doping sources. The resulting 3D BNC NRs possess abundant edges, thin walls, tunable BN content, and multilevel porous structures. Such unique features not only provide a large amount of active sites for ORR but also are favorable for the fast transport of oxygen and reduction

Received: October 12, 2014
Revised: January 30, 2015
Published: February 2, 2015

DOI: 10.1021/cm5037502
Chem. Mater. 2015, 27, 1181−1186

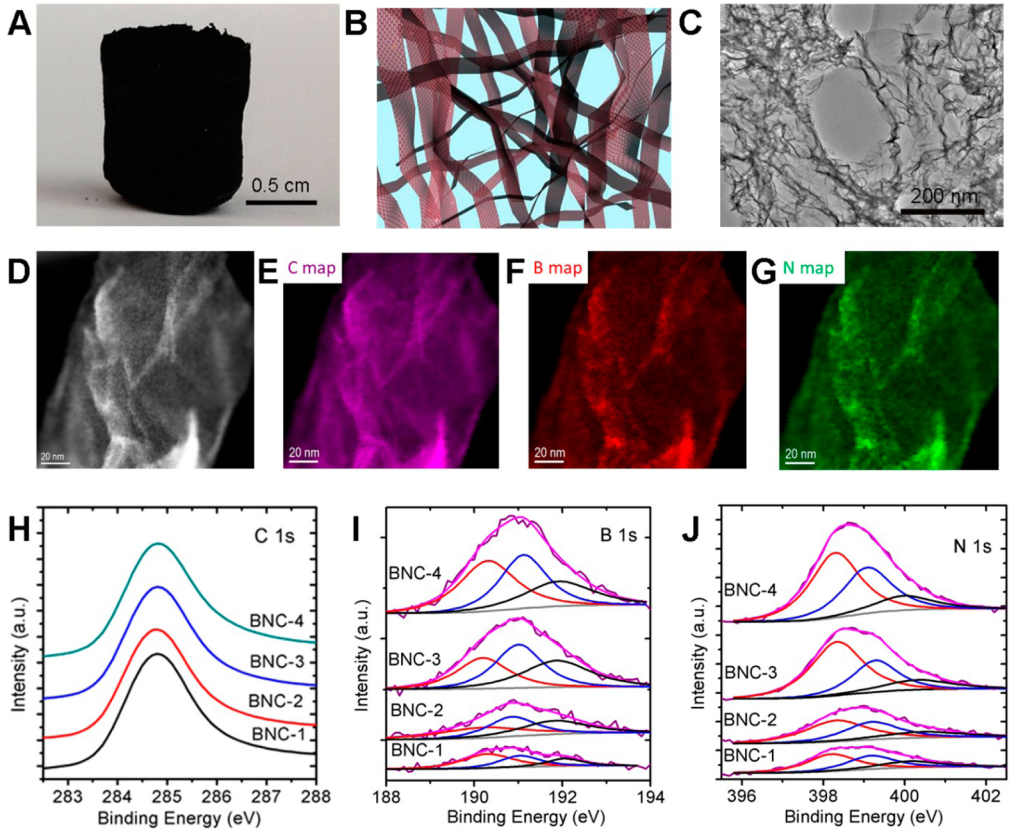

Figure 1. Structure characterization of the BNC nanoribbon electrocatalysts. (A) Photograph showing the morphology of BNC NR aerogels. (B) Schematic diagram of 3D BNC NR aerogels. (C) TEM image of the BNC NR aerogels showing its 3D porous structure. (D) STEM ADF image of BNC NR with ~10 atom % BN and the corresponding elemental mapping of (E) carbon, (F) boron, and (G) nitrogen. High-resolution XPS spectra of (H) C 1s, (I) B 1s, and (J) N 1s from BNC NR aerogels with different B/N substitution levels from 5.9 atom % to 24.2 atom %.

Table 1. Concentration of Boron, Nitrogen, and Carbon in Different BNC NR Samples

material (atom %)	BNC-1	BNC-2	BNC-3	BNC-4
carbon	94.1	90.3	83.6	75.8
boron	2.8	4.7	8.1	11.9
nitrogen	3.1	5.0	8.3	12.3

products. As a consequence, BNC architectures with BN content of ~10 atom % exhibit excellent ORR electrocatalytic properties, including high electrocatalytic activity, long-term durability, and high selectivity. Remarkably, this catalyst possesses the highest onset and half-wave potentials for ORR in alkaline media of any reported metal-free catalyst, and even outperforms the most active Pt−C catalyst.

As illustrated in Supporting Information Figure S1, the synthesis procedure to 3D BNC NRs involves three steps. First, water-dispersible GONR was synthesized by unzipping multi-walled carbon nanotubes under oxidation conditions.[20] The as-prepared GONR was then used as building block to construct 3D GONR architectures via a cross-linking reaction at 180 °C in an autoclave, similar to the formation of 3D graphene oxide hydrogels.[21] After freeze-drying, the samples were annealed with boric acid and ammonia at 1000 °C, where GONRs were thermally reduced to graphene nanoribbons (GNRs), and at the same time boron and nitrogen were codoped into the GONRs, creating 3D BNC NRs (for the details, see Experimental Methods in Supporting Information). Notably, the BN content in the resulting materials was controllably adjusted from 5.9 atom % to 24.2 atom % (for detailed composition of each sample, see Table 1). BNC-1, BNC-2, BNC-3, and BNC-4 correspond to annealing times of 15 min, 30 min, 45 min, and 1 h, respectively. The oxygen percent is very low and ignored here. The BNC NR products can be produced in large volume with low volume densities of ~10 mg/cm^3 (Figure 1A), and Figure 1B is the typical schematic showing its porous structure.

The structure and morphology of as-prepared BNC NRs were investigated by scanning electron microscopy (SEM) and transmission electron microscopy (TEM). As shown in Figures 1C and Supporting Information Figure S2, the 3D interpenetrating networks built from numerous flexible ribbons are clearly visible. The lateral sizes of the building block ribbons are typically in the range of tens of nanometers in width and several tens of micrometers in length (Figure 1C). Their adsorption−desorption isotherms exhibit a typical IV hysteresis loop at a relative pressure between 0.4 and 1.0 (Supporting Information Figure S3), characteristic of pores with different pore sizes. In a typical case of BNC NR with ~10 atom % BN doping content, a high specific surface area of 875 m^2/g is observed from the adsorption data. This value is much higher than that of the directly dried GONR powder (201 m^2/g) (Supporting Information Figures S3 and S4), further demonstrating that our controllable assembly strategy is an efficient protocol to prevent the restacking of GNRs. Figure 1D−G shows a typical scanning transmission electron microscopy (STEM) annular dark field (ADF) image and elemental mapping of BNC NR with ~10 atom % BN, where all the elements (B, C, and N) are

DOI: 10.1021/cm5037502
Chem. Mater. 2015, 27, 1181−1186

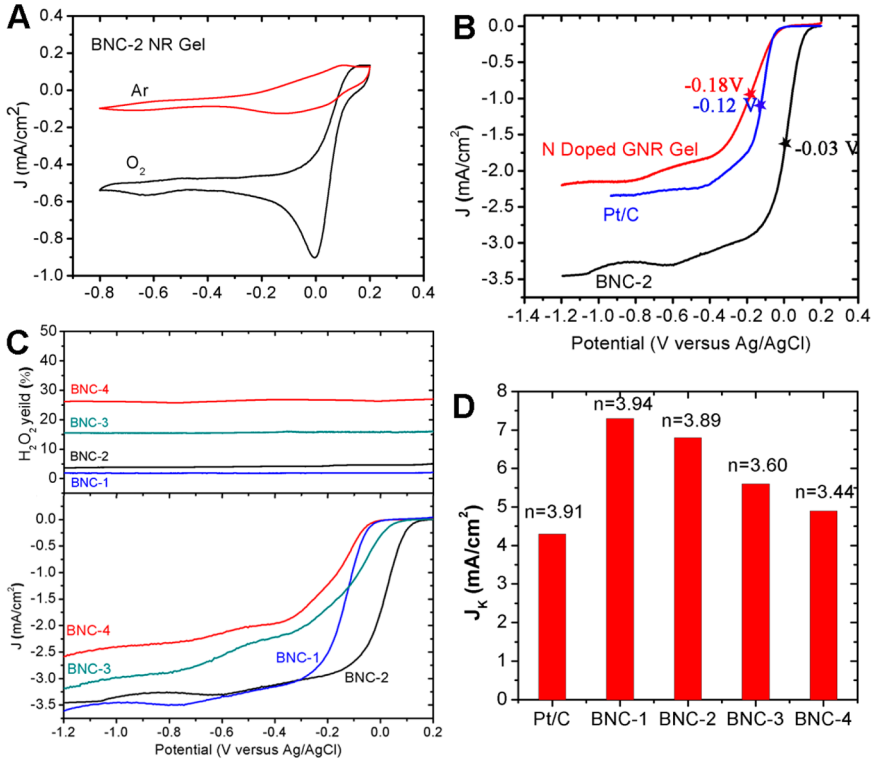

Figure 2. Electrocatalytic characterization of BNC NR aerogels with different doping concentrations of BN. (A) CVs of BNC-2 NR catalyst in O_2- or Ar-saturated 0.1 M KOH electrolyte. (B) Disk current densities of the RRDE versus potential derived from BNC-2, N-doped GNR aerogels, and commercial Pt/C catalyst. (C) Disk current densities of the RRDE versus potential derived from BNC NR aerogels with different compositions in oxygen-saturated 0.1 M KOH, also with the corresponding H_2O_2 percentage of each sample calculated from the RRDE disk and ring current. (D) Comparison of the ORR performances of different BNC NR aerogels and commercial Pt/C catalyst in kinetic current densities (J_K) and electron transfer number (n).

homogeneously distributed throughout the whole NR. The electron energy loss spectroscopy (EELS) (Supporting Information Figure S2E) and X-ray photoelectron spectroscopy (XPS) (Figure 1H-1J, Supporting Information Figure S5) analysis further shows that carbon, boron, nitrogen, and oxygen are present in the BNC NR, and the BN content can be tailored by controlling the duration of the annealing process under boron and nitrogen environment (Table 1). The complex B 1s spectra can be further deconvoluted into three different components with binding energies of 190.3, 191.1, and 191.9 eV, attributed to BNC_2, BN_2C, and BN_3, respectively.[22] Correspondingly, the N 1s spectra can be fitted with three peaks at 398.3, 399.1, and 400.0 eV, ascribed to NB_3, NB_2C, and NBC_2, respectively.[22] Upon increasing the annealing time from 15 min to 1 h, the signals for BN_3 and NB_3 significantly increase, suggesting the aggregation of BN pairs into BN domains at high BN concentration.[23,24] In addition, the substitutional doping is supported by the increase of the D peak in the Raman spectra from the converted BNC NR (Supporting Information Figure S6).

The electrocatalytic activity of BNC NR for ORR was initially examined by cyclic voltammetry (CV) in the potential range from 0.2 to −1.0 V vs Ag/AgCl at a scan rate of 100 mV/s. As shown in Figure 2A, in the Ar-saturated 0.1 M KOH solution, a featureless voltammogram without any evident peak is observed. In contrast, as the KOH solution is saturated with O_2, a well-defined and strong cathodic peak occurs at about 0 V, indicating the high catalytic activities of BNC NR for ORR. More importantly, this cathodic peak is even more positive than that of commercially available Pt/C catalyst (−0.2 V) (Supporting Information Figure S7A). To gain further insights into the ORR activity of BNC NR, rotating ring disk electrode (RRDE) voltammetry was performed in O_2-saturated 0.1 M KOH solution at a scanning rate of 10 mV/s (Figure 2B,C and Supporting Information Figure S7B). The electrocatalytic properties including the onset potential, half-wave potential, saturated current density, and electron transfer number are strongly dependent on B and N doping concentrations in BNC NR. As shown in Figure 2C and Supporting Information Figure S8, with an increase of the doping level from 5.9 atom % to 24.2 atom %, the onset potential first increases and then decreases with the highest value of 0.1 V vs Ag/AgCl (1.09 V vs RHE, Supporting Information Figure S8A) for BNC-2 with ∼10 atom % BN content. More remarkably, the half-wave potential of BNC-2 is only −0.03 V vs Ag/AgCl (0.96 V vs RHE) (Figure 2B), which is higher than any reported metal-free catalyst in alkaline media (0.4 to 0.8 V vs RHE)[2,8,25−27] and even higher than commercial Pt−C catalysts (0.87 V vs RHE in this study). To avoid any problem caused by using the Ag/AgCl reference in alkaline solution (chloride contamination), Hg/HgO reference was also used to test the RRDE voltammetry curves of BNC-2 and commercial Pt−C catalysts (Supporting Information Figure S9), and the same conclusions can be made. On the basis of the above data, BNC-2 has much better electrocatalytic performance than N-doped GNRs. Such high onset potential and half-wave potential could give rise to a very low overpotential.

From the RRDE voltammograms, the production of peroxide species (HO_2^-) during the ORR process can also be identified. It is striking that the HO_2^- yields are less than 5% for the BNC

DOI: 10.1021/cm5037502
Chem. Mater. 2015, 27, 1181−1186

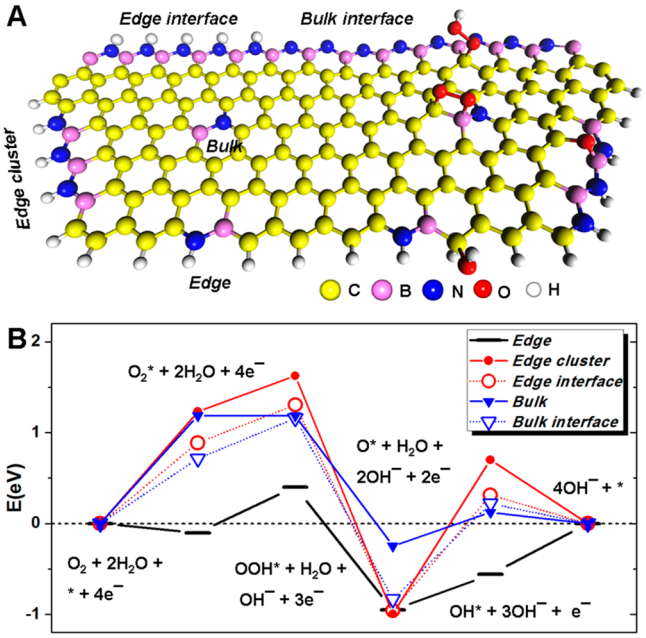

Figure 3. Theoretical simulations. (A) Schematic representations of structural models along with some selected intermediate states. The interface (a line of zigzag BN chains) could either simply represent the bulk interface where the BN and graphene domains meet or be saturated by hydrogen atoms forming the edge interface. (B) Free energy diagram for ORR on different models for comparison under the conditions of pH = 13 and the maximum potential allowed by thermodynamics. The proposed associative mechanism involves the following steps: (1) $O_2 + 2H_2O + * + 4e^- \rightarrow O_2* + 2H_2O + 4e^-$;(2) $O_2* + 2H_2O + 4e^- \rightarrow OOH* + H_2O + OH^- + 3e^-$; (3) $OOH* + H_2O + OH^- + 3e^- \rightarrow O* + H_2O + 2OH^- + 2e^-$; (4) $O*+ H_2O + 2OH^- + 2e^- \rightarrow OH* + 3OH^- + e^-$; (5) $OH* + 3OH^- + e^- \rightarrow 4OH^- + *$, where * denotes an active site on the catalyst surface.

NR with BN content ranging from 6 atom % to 10 atom % (Figure 2C and Supporting Information Figure S10). This value is close to that of commercial Pt–C catalysts (4–5%), suggesting that these BNC NRs exhibit mainly a one-step, four-electron transfer pathway for ORR. The kinetic parameters, including electron transfer number (n) and kinetic current density (J_K) of the resulting BNC NR (Figure 2D), were further analyzed on the basis of the Koutecky–Levich eqs (Supporting Information Figure S11) and eq 1.

$$n = 4I_D/(I_D + I_R/N) \quad (1)$$

where $N = 0.36$ is the current collection efficiency, I_D is the disk current, and I_R is the ring current. An electron transfer number of ~3.9 is achieved for the BNC NR with the BN content ranging from 5.9 atom % to 9.7 atom %, in good agreement with the above analysis. However, with the increase of BN content from 16.4 atom % to 24.2 atom %, the electron transfer number of the BNC NR is reduced from 3.6 to 3.2, involving mixed two-electron and four-electron transfer pathways during the ORR process. The decrease of the electron transfer number can be attributed to the reduction of the electrical conductivity with increasing BN content,[24] obstructing electron transfer from electrode to the oxygen atoms or molecular. The kinetic current density of BNC NR is also strongly governed by the BN content. Typically, the highest kinetic current density of 7.2 mA/cm^2 is observed for BNC-1. This value is much higher than that of commercial Pt/C (J_K = 4.3 mA/cm^2) under the same testing conditions. Overall, the catalytic activity increases at the beginning and then decreases with the increase of BN content, which can be explained by the change in the number of catalytically active sites and electrical conductivity of the BNC NR. At the beginning, increasing the BN concentration (<10%) results in more catalytic sites, leading to the improvement of their catalytic activity, which is consistent with the previously reported work on nitrogen doped GNR.[28] However, further increasing the doping concentration (>10%) would undermine the conductivity of BNC, which would weaken the charge transport from electrode to oxygen.

To shed light on the ORR catalytic behaviors of BNC NRs with various BN contents, spin-polarized density functional theory (DFT) calculations were performed using the Vienna ab initio Simulation Package (VASP).[29] Five configurations, (i) one BN pair in the middle of a graphene sheet (*Bulk*), (ii) one BN pair at the edge (*Edge*), (iii) three BN pairs at the edge (*Edge cluster*), (iv) a line of BN pairs at the nanoribbon edges (*Edge interface*), and (v) the interface between BN and graphene domains (*Bulk interface*), representing different doping concentrations, are shown in Figure 3A. As proposed by Bao et al., O_2 reduction in alkaline solution follows the associative rather than the dissociative mechanism.[30] The free

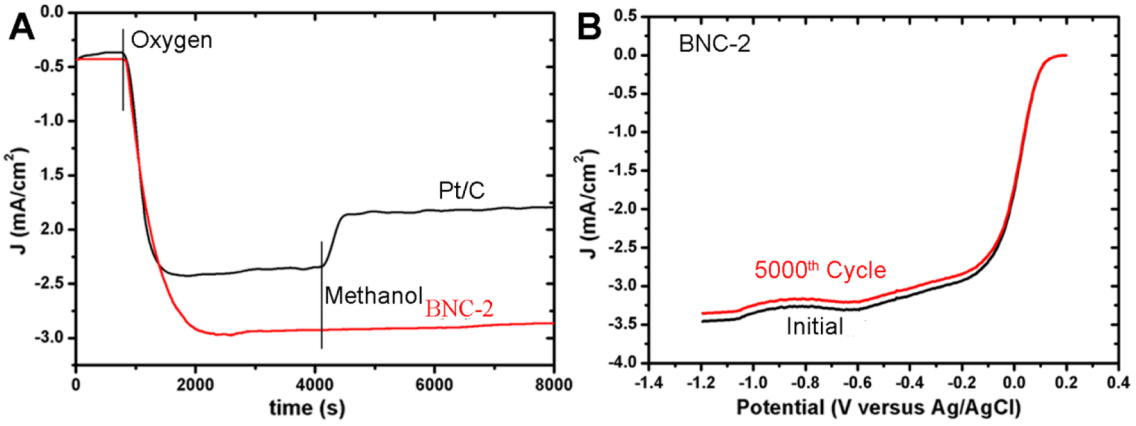

Figure 4. ORR performances of BNC-2 NR aerogel catalyst for assessment of methanol tolerance and durability. (A) Current density–time responses at −0.4 V in 0.1 M KOH on BNC-2 and Pt–C electrode (900 rpm) followed by introduction of O_2 and methanol (0.3 M). (B) Cycle performance of BNC-2 before and after 5000 potential cycles in O_2-saturated 0.1 M KOH.

DOI: 10.1021/cm5037502
Chem. Mater. 2015, 27, 1181–1186

energy diagrams (Figure 3B) clearly show that, in the case of *Bulk* doping, the highest energy barrier is 1.18 eV for O_2 adsorption, which is identified as the rate-determining step. In sharp contrast, with the introduction of one BN pair at the GNR edges (*Edge*), the O_2 adsorption becomes energetically favorable. With further increasing the BN doping level, *h*-BN domains tend to nucleate and grow in the GNRs,[22] forming finite *Edge cluster*, *Edge interface*, or *Bulk interface* (note that for *Edge cluster* case we consider the active C site bonding to the middle B site to make a difference from the *Edge* case). Our simulations demonstrate that not only the binding of O_2 for all these three cases remains a steep uphill process, but also the barriers for proton transfer to adsorbed O are larger than 1 eV, indicating weak OH binding relative to the strong O binding. For the *Edge* case, the binding between the OH and edge C next to the B atom, where the π bonding in graphene is partially broken, renders the bond hybridization of the C atom changing from sp^2 to sp^3 (bottom right in Figure 3A). This makes the energy for OH adsorption and the barrier for the O protonation decrease significantly. Thus, the decreased number of such edge C sites, the increased barriers for the two rate-determining steps at the interfaces, and the reduced electrical conductivity clearly explain the above electrocatalytic activity change as doping concentration varies from 5.9 atom % to 24.2 atom %. Further analyses show that the spin polarization of the edge C atoms near active B sites plays a key role in the enhancement of the binding of O_2 (see detailed discussions in Supporting Information). The comparative study on the isolated B- or N-doping in graphene matrix or edge (Supporting Information Figure S17) further corroborates that it is BN edge codoping rather than isolated B/N doping that plays a dominant role in enhancing the ORR performance.

To evaluate the properties of a new electrocatalyst for ORR, the crossover effect should also be considered, since the fuel in the anode, such as methanol or glucose, might permeate through the polymer membrane to the cathode and seriously affect the performance of the ORR catalysts. Thus, the electrocatalytic sensitivity of BNC-2 NRs and commercial Pt/C catalysts were measured against the electro-oxidation of methanol in ORR. As shown in Figure 4A, current density−time responses were used to detect the effect of oxygen and methanol. Both of them have a strong response to O_2; however, a significant decrease in current density is observed for the Pt/C catalyst in O_2-saturated 0.1 M KOH solution when 3 M methanol is added, whereas no noticeable response for BNC-2 NRs is detected. Apparently, BNC-2 NRs show a good selectivity for ORR and, thus, a remarkably better tolerance of crossover effect against methanol than commercial Pt/C catalysts. More importantly, the durability of the BNC architecture is much better than that of Pt−C. As shown in Figure 4B, after 5000 continuous cycles, both the onset potential and the half-wave potential almost overlap with the first cycle, demonstrating the excellent durability of the BNC NR for ORR.

In summary, we have demonstrated that optimally doped boron and nitrogen in graphene nanoribbons show excellent ORR electrocatalytic activity, even better than the commercial Pt−C catalysts. The high activity, excellent tolerance to methanol, high durability, and superior high half-wave potential are achieved for optimally doped (10 atom % BN) BNC NR catalysts in comparison to other metal-free catalysts in alkaline solution. The new BNC catalysts could serve as efficient metal-free ORR electrocatalysts for fuel cells and other electrochemical and catalytic applications.

■ ASSOCIATED CONTENT

Supporting Information

Methods, characterizations, and theory simulations are included. This material is available free of charge via the Internet at http://pubs.acs.org.

■ AUTHOR INFORMATION

Corresponding Authors

*E-mail: (S.Y.) yangshubin@buaa.edu.cn.
*E-mail: (J.M.T.) tour@rice.edu.
*E-mail: (P.M.A.) ajayan@rice.edu.

Author Contributions

Y.G., H.F., and S.Y. designed and carried out most of the experiments and analyzed the data. X.Z. proposed the reaction mechanism and performed the theoretical part. W.Z. carried out STEM experiments, with partial input from Z.L. and Z.P. G.Y. worked on part of the ORR test. Y.G., H.F., S.Y., X.Z., W.Z., J.M.T., and P.M.A. cowrote the paper.

Author Contributions

#(Y.G., H.F., X.Z.) These authors contributed equally to this work.

Notes

The authors declare no competing financial interest.

■ ACKNOWLEDGMENTS

This work was supported by the Welch Foundation Grant C-1716, the NSF Grant DMR-0928297, the U.S. Army Research Office MURI Grant W911NF-11-1-0362, The Air Force Office of Scientific Research Grant FA9550-09-1-0581, The Air Force Office of Scientific Research MURI Grant FA9550-12-1-0035, and the Office of Naval Research MURI Grant N000014-09-1-1066. The computations were performed at the Cyberinfrastructure for Computational Research funded by NSF under Grant CNS-0821727 and the Data Analysis and Visualization Cyberinfrastructure funded by NSF under Grant OCI-0959097. This research was also supported in part by a Wigner Fellowship through the Laboratory Directed Research and Development Program of Oak Ridge National Laboratory (ORNL), managed by UT-Battelle, LLC, for the U.S. DOE (WZ), and through a user project supported by ORNL's Center for Nanophase Materials Sciences (CNMS), which is sponsored by the Scientific User Facilities Division, Office of Basic Energy Sciences, U.S. DOE.

■ REFERENCES

(1) Gong, K. P.; Du, F.; Xia, Z. H.; Durstock, M.; Dai, L. M. *Science* **2009**, *323*, 760.
(2) Li, Y. G.; Zhou, W.; Wang, H. L.; Xie, L. M.; Liang, Y. Y.; Wei, F.; Idrobo, J. C.; Pennycook, S. J.; Dai, H. J. *Nat. Nanotechnol.* **2012**, *7*, 394.
(3) Xiong, W.; Du, F.; Liu, Y.; Perez, A.; Supp, M.; Ramakrishnan, T. S.; Dai, L. M.; Jiang, L. *J. Am. Chem. Soc.* **2010**, *132*, 15839.
(4) Wu, G.; More, K. L.; Johnston, C. M.; Zelenay, P. *Science* **2011**, *332*, 443.
(5) Debe, M. K. *Nature* **2012**, *486*, 43.
(6) Stamenkovic, V. R.; Fowler, B.; Mun, B. S.; Wang, G. F.; Ross, P. N.; Lucas, C. A.; Markovic, N. M. *Science* **2007**, *315*, 493.
(7) Winther-Jensen, B.; Winther-Jensen, O.; Forsyth, M.; MacFarlane, D. R. *Science* **2008**, *321*, 671.
(8) Qu, L. T.; Liu, Y.; Baek, J. B.; Dai, L. M. *ACS Nano* **2010**, *4*, 1321.

DOI: 10.1021/cm5037502
Chem. Mater. 2015, 27, 1181−1186

(9) Yang, S. B.; Feng, X. L.; Wang, X. C.; Müllen, K. *Angew. Chem., Int. Ed.* **2011**, *50*, 5339.
(10) Liang, J.; Jiao, Y.; Jaroniec, M.; Qiao, S. Z. *Angew. Chem., Int. Ed.* **2012**, *51*, 11496.
(11) Yang, Z.; Yao, Z.; Li, G. F.; Fang, G. Y.; Nie, H. G.; Liu, Z.; Zhou, X. M.; Chen, X.; Huang, S. M. *ACS Nano* **2012**, *6*, 205.
(12) Zhang, C.; Mahmood, N.; Yin, H.; Liu, F.; Hou, Y. *Adv. Mater.* **2013**, *25*, 4932.
(13) Gasteiger, H. A.; Kocha, S. S.; Sompalli, B.; Wagner, F. T. *Appl. Catal., B* **2005**, *56*, 9.
(14) Liang, Y. Y.; Li, Y. G.; Wang, H. L.; Zhou, J. G.; Wang, J.; Regier, T.; Dai, H. J. *Nat. Mater.* **2011**, *10*, 780.
(15) Paulus, U. A.; Wokaun, A.; Scherer, G. G.; Schmidt, T. J.; Stamenkovic, V.; Markovic, N. M.; Ross, P. N. *Electrochim. Acta* **2002**, *47*, 3787.
(16) Paraknowitsch, J. P.; Thomas, A. *Energy Environ. Sci.* **2013**, *6*, 2839.
(17) Maldonado, S.; Stevenson, K. J. *J. Phys. Chem. B* **2005**, *109*, 4707.
(18) Fan, X. F.; Zheng, W. T.; Kuo, J. L. *RSC Adv.* **2013**, *3*, 5498.
(19) Kim, H.; Lee, K.; Woo, S. I.; Jung, Y. *Phys. Chem. Chem. Phys.* **2011**, *13*, 17505.
(20) Higginbotham, A. L.; Kosynkin, D. V.; Sinitskii, A.; Sun, Z. Z.; Tour, J. M. *ACS Nano* **2010**, *4*, 2059.
(21) Zhang, L.; Shi, G. Q. *J. Phys. Chem. C* **2011**, *115*, 17206.
(22) Ci, L.; Song, L.; Jin, C. H.; Jariwala, D.; Wu, D. X.; Li, Y. J.; Srivastava, A.; Wang, Z. F.; Storr, K.; Balicas, L.; Liu, F.; Ajayan, P. M. *Nat. Mater.* **2010**, *9*, 430.
(23) Lin, T. W.; Su, C. Y.; Zhang, X. Q.; Zhang, W. J.; Lee, Y. H.; Chu, C. W.; Lin, H. Y.; Chang, M. T.; Chen, F. R.; Li, L. J. *Small* **2012**, *8*, 1384.
(24) Gong, Y. J.; Shi, G.; Zhang, Z. H.; Zhou, W.; Jung, J.; Gao, W. L.; Ma, L. L.; Yang, Y.; Yang, S. B.; You, G.; Vajtai, R.; Xu, Q. F.; MacDonald, A. H.; Yakobson, B. I.; Lou, J.; Liu, Z.; Ajayan, P. M. *Nat. Commun.* **2014**, *5*, 3193.
(25) Yang, L. J.; Jiang, S. J.; Zhao, Y.; Zhu, L.; Chen, S.; Wang, X. Z.; Wu, Q.; Ma, J.; Ma, Y. W.; Hu, Z. *Angew. Chem., Int. Ed.* **2011**, *50*, 7132.
(26) Chen, S.; Bi, J. Y.; Zhao, Y.; Yang, L. J.; Zhang, C.; Ma, Y. W.; Wu, Q.; Wang, X. Z.; Hu, Z. *Adv. Mater.* **2012**, *24*, 5593.
(27) Wang, S. Y.; Yu, D. S.; Dai, L. M. *J. Am. Chem. Soc.* **2011**, *133*, 5182.
(28) Liu, M. K.; Song, Y. F.; He, S. X.; Tjiu, W. W.; Pan, J. S.; Xia, Y. Y.; Liu, T. X. *ACS Appl. Mater. Interfaces* **2014**, *6*, 4214.
(29) Kresse, G.; Furthmuller, J. *Phys. Rev. B* **1996**, *54*, 11169.
(30) Yu, L.; Pan, X. L.; Cao, X. M.; Hu, P.; Bao, X. H. *J. Catal.* **2011**, *282*, 183.

DOI: 10.1021/cm5037502
Chem. Mater. 2015, 27, 1181−1186